Volume 59
Number 41
21 May 2023
Pages 6099–6260

ChemComm

Chemical Communications

rsc.li/chemcomm

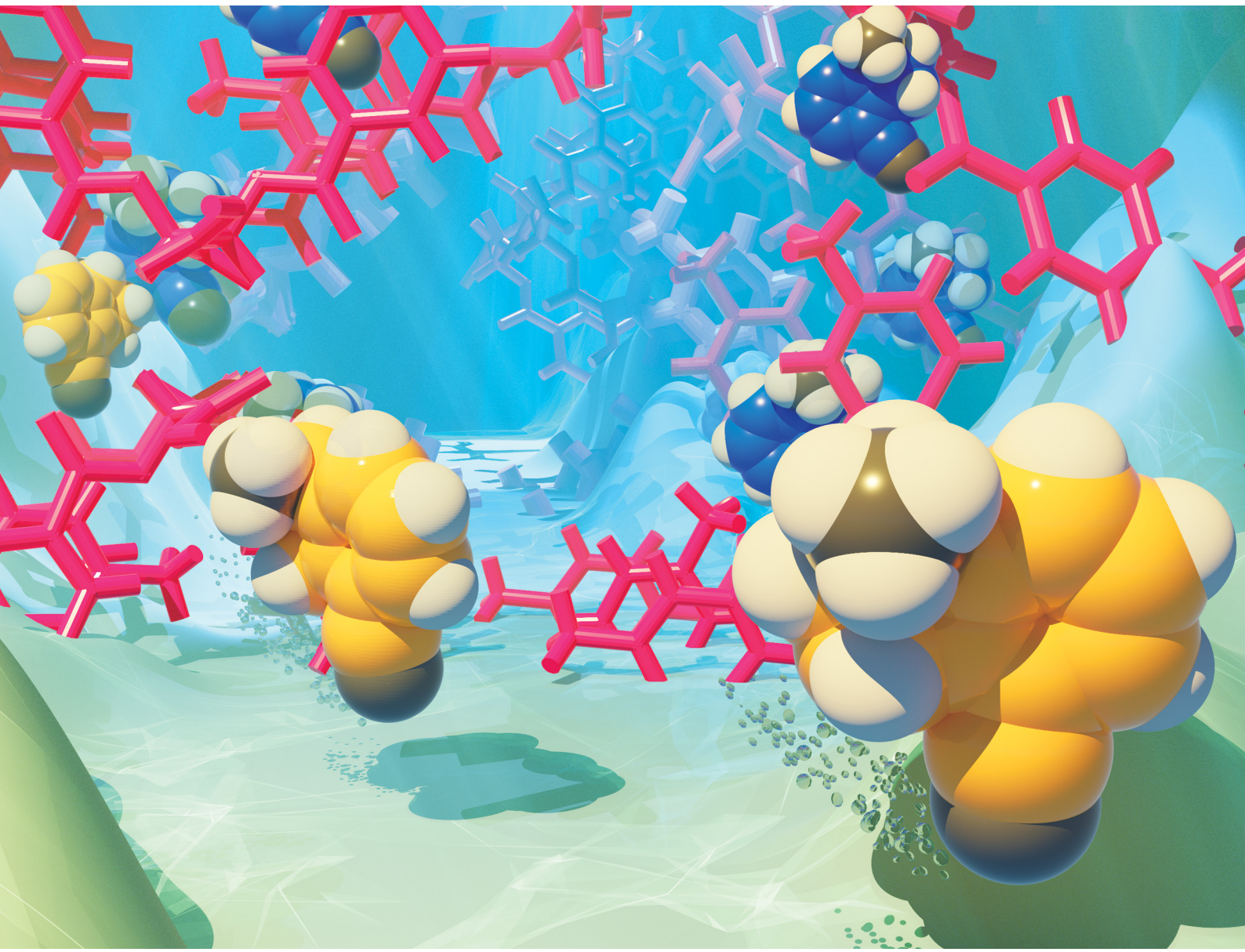

ISSN 1359-7345

ROYAL SOCIETY OF CHEMISTRY

COMMUNICATION

Ryusei Oketani, Ichiro Hisaki *et al.*

Overcoming a solid solution system on chiral resolution: combining crystallization and enantioselective dissolution

ChemComm

COMMUNICATION

View Article Online
View Journal | View Issue

Cite this: *Chem. Commun.*, 2023, 59, 6175

Received 20th March 2023,
Accepted 17th April 2023

DOI: 10.1039/d3cc01352a

rsc.li/chemcomm

Overcoming a solid solution system on chiral resolution: combining crystallization and enantioselective dissolution†

Ryusei Oketani, *‡ Koki Shiohara‡ and Ichiro Hisaki *

Chiral resolution of rac-4-cyano-1-aminoindane, a key intermediate of ozanimod, was successfully achieved through a combination of crystallization and enantioselective dissolution with up to 96% ee. The disastereomeric salt with di-*p*-toluoyl-L-tartaric acid was characterized by the construction of a binary phase diagram and ternary isotherm. Enantioselective dissolution was then employed to further enrich the enantiomer.

The chirality of active pharmaceutical ingredients is of great importance in the fields of chemistry and life sciences. For example, the anti-malarial drug mefloquine shows significant differences in properties between its two enantiomers: (+)-(11*S*,12*R*)-mefloquine acts as an effective anti-malarial drug whereas (−)-(11*R*, 12*S*)-mefloquine causes side effects on the central nervous system.[1] Therefore, it is important to separate the two enantiomers and investigate their respective properties. In this context, chiral resolution by crystallization methods such as preferential crystallization,[2] diastereomeric salt formation,[3] co-crystallization[4] and deracemization[5] has been widely utilized due to its economic advantages and simplicity of operation. However, these methods require crystallization conditions that yield precipitates containing only the desired enantiomer, such as in a eutectic system. As a result, the formation of solid solutions with non-stoichiometric compositions is recognized as one of the significant challenges in chiral resolution (Fig. 1a). Although solid solutions are not frequently observed according to the statistics, it is difficult to identify the crystal structure when encountered, because a solid solution appears to be of a single composition in X-ray structural analysis or other analytical techniques. In practice, this can be determined by constructing a phase diagram using thermal analysis at various compositions, *i.e.*, a solid solution system exhibits a continuous change in melting point or solubility along with the composition change (Fig. 1a).

Herein, we report a new chiral resolution method for addressing solid solution crystals by combining crystallization and enantioselective dissolution. We discovered that the key intermediate of ozanimod (ZEPOSIA®), 4-cyano-1-aminoindane **1**, forms a diastereomeric complete solid solution with di-*p*-toluoyl-L-tartaric acid, and chiral resolution was successfully achieved based on phase diagram studies and enantioselective dissolution. Access to enantiopure *S*-**1** has been achieved by asymmetric synthesis using chiral Ellman's auxiliary[6] and enzymatic methods.[7] However, while salt formation with tartaric acid has been described,[8] the chiral resolution of the racemic form and its crystal structure have not yet been reported. In this approach, after purification to moderate optical purity by thermodynamic equilibrium in a complete solid solution of the diastereomeric pair, the kinetically metastable diastereomeric pair is dissolved by immersing in the solvent for a short time. This combination overcomes the optical purity of the solid solution achieved by thermodynamic equilibrium (Fig. 1b). The synthesis of **1** was carried out in seven steps from naphthalene with some modifications to the method described by Uttoff and co-workers.[7] Crystallization of racemic **1** and di-*p*-toluoyl-L-tartaric acid was performed from a methanol solution to yield single crystals. Single crystal X-ray analysis revealed a crystal structure of the diastereomeric salt composed of *S*-**1** and L-acid with the composition ratio of *S* and *R* isomers of 87/13, as shown in Fig. 2. In the crystal structure, the amine moiety of **1** was fully protonated regardless of its chirality and one of the carboxylic acids on the tartaric acid was deprotonated, while the other one remained protonated (Fig. 2a).

The charge-assisted hydrogen bonding was confirmed between the amine and acid with an NH/O distance of 2.67 Å. The overall stoichiometric ratio of **1** : L-acid is 1 : 1. The ammonium and the carboxylate formed a columnar structure with a 2-fold axis along the *a*-axis (Fig. 2b and c). The carboxylic acid

Division of Chemistry, Graduate School of Engineering Science, Osaka University, 1-3 Machikaneyama, Toyonaka, Osaka 560-8531, Japan.
E-mail: r.oketani.es@osaka-u.ac.jp, i.hisaki.es@osaka-u.ac.jp

† Electronic supplementary information (ESI) available: Details of synthesis, crystallographic data, thermal analysis, theoretical calculations, and experimental procedure of chiral resolution. CCDC 2236669. For ESI and crystallographic data in CIF or other electronic format see DOI: **https://doi.org/10.1039/d3cc01352a**

‡ These authors equally contributed to the work. All the authors agreed to switch the order of the first and second authors in their respective CVs.

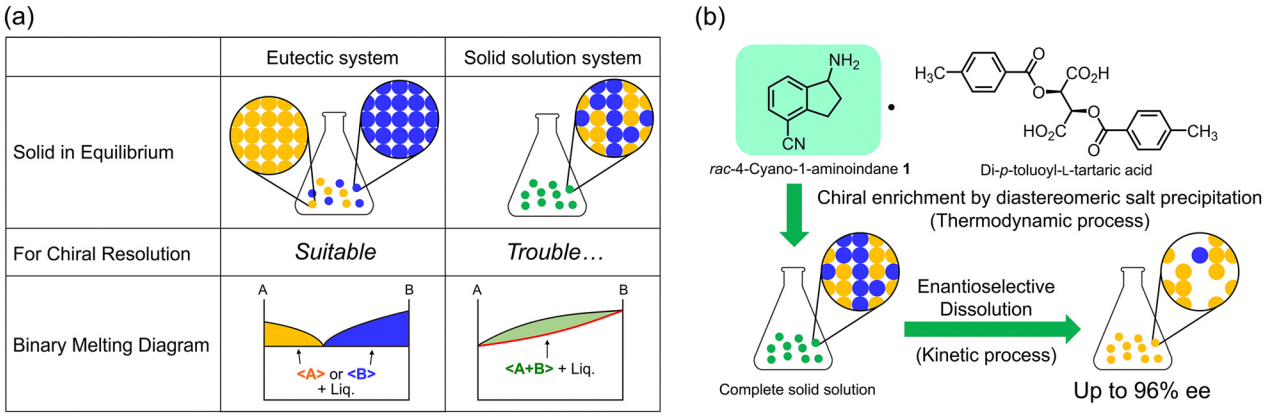

Fig. 1 (a) Categories of solid phases for racemates and their applicability in chiral resolution. In the binary melting diagram, ⟨A⟩, ⟨B⟩, and ⟨A + B⟩ represent the crystalline solids of each component. The colored domains indicate the components at thermodynamic equilibrium. The red line shows the melting points along the composition change. (b) Chiral resolution of the aminoindane derivative **1** through enantio-enriched diastereomeric salt precipitation with di-*p*-toluoyl-L-tartaric acid and subsequent enantioselective dissolution.

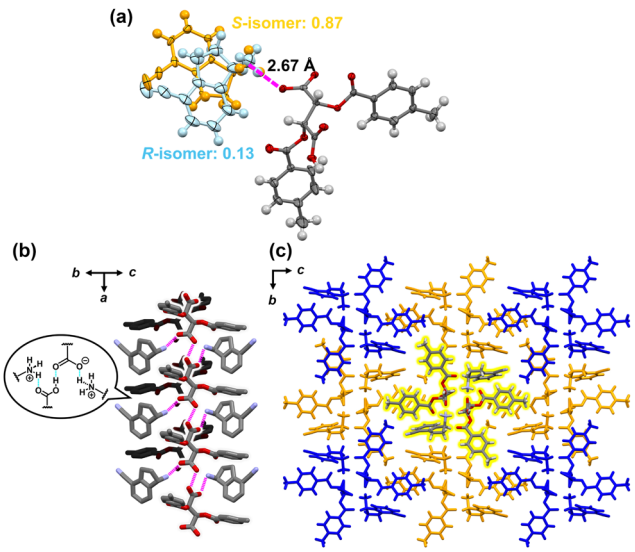

Fig. 2 The crystal structure of **1**·L-acid salt. (a) The components in the ellipsoids with a 50% probability level. The occupancy ratio of two enantiomers is *S*/*R* = 87/13. (b) The charge-assisted hydrogen bonding between the ammonium and carboxylic acid groups. *R*-isomers are omitted for clarity. (c) The packing structure viewed along the *a*-axis. Models in the same color correspond to a single columnar structure.

formed a hydrogen bond with the neighboring carboxylate. The negative charge per molecule of tartaric acid was 1, suggesting that the charge was not localized to one carboxylic acid and might be delocalized across both of the carboxylic acids. The average bond lengths of C–O and C=O on carboxyl groups were 1.25 and 1.26 Å, indicating that these groups are in a similar environment.

Interestingly, the ee varied in the bulk sample and 56% ee was obtained for the entire sample. Noatbly, the ee in the crystals was never close to 100% in a single crystallization, even when the solution was manipulated to avoid drying up during crystallization. In general, ideal diastereomeric salts give a eutectic mixture, allowing the optical purity to be close to 100%. In the present system, crystal structures somewhat enriched with the *S*-isomer were obtained, but the presence of the *R*-isomer was identified as a disordered structure. These findings suggest that this system forms a solid solution and further investigation of the crystallization is required to achieve efficient chiral resolution.

The true solid-state landscape of the salt can be revealed by constructing a melting point phase diagram and a ternary isotherm including solvents. The binary melting phase diagram of *S*-**1** : L-acid (**SL**) and *R*-**1** : L-acid (**RL**) was constructed using DSC measurements and PXRD measurements. Crystalline solids with different compositions were prepared by repeatedly crystallizing crystals containing **1** and L-acid. The crystals were gradually enriched to **SL**, whereas the solution phase was enriched toward **RL**; the crystalline phase with an excess of **RL** was obtained by evaporating the solution phase remaining from the previous crystallization.

The onset and peak temperatures in DSC measurements, corresponding to solidus and liquidus, respectively, were distributed between 186 °C and 215 °C as shown in Fig. 3a and Fig. S5 (ESI†). These temperatures increased with enrichment of **SL** and no clear eutectic point could be detected. This is typical behavior of the complete solid solution. The higher melting point in **SL**-enriched solids also indicated that **SL** is a more stable form than **RL**. This is consistent with the crystallization behavior of rac-**1** and L-acid, which yield *S*-enriched crystals. The difference of intermolecular interaction energy between the two diastereomers also supports the relative stability of **SL** against **RL** (Fig. S8, ESI†). Compound **1** is a waxy solid at room temperature, melts at 60 °C, and begins to decompose or sublime around 150 to 170 °C (Fig. S6, ESI†). This means that the decomposition of **1** is observed in the thermal events simultaneously with the fusion of the salt crystals. In the PXRD measurements, most of the peaks are identical despite the various compositions (Fig. 3b). However, some peaks change slightly in 2-θ position with compositional changes.

The intensity of a peak at 13.7° gradually decreases with the enrichment of **RL**. This peak can be assigned to the diffraction

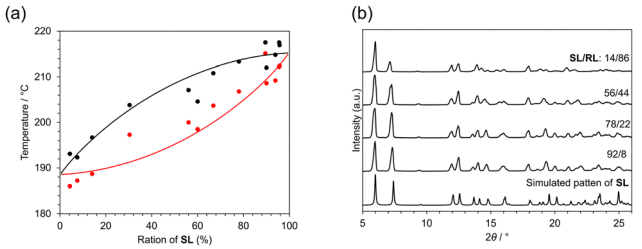

Fig. 3 (a) The binary melting phase diagram of **SL** and **RL**. Red symbols indicate onset temperatures of the first thermal event, corresponding to the solidus. Black symbols indicate peak temperatures of the melting upon heating, corresponding to the liquidus. (b) The PXRD patterns of the solid with various compositions of *R*- and *S*-isomers. All compositions are determined by HPLC analysis.

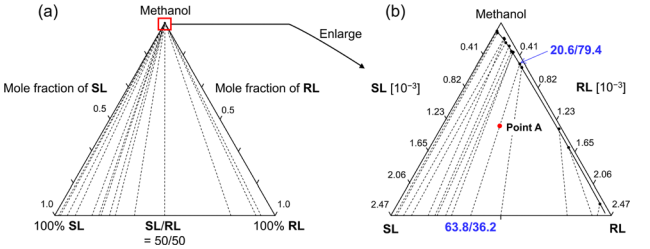

Fig. 4 The ternary isotherm of **SL**/**RL**/MeOH at 20 °C: (a) The whole projection. (b) The enlarged projection of the square region in the phase diagram offering a closer look at the solubilities and compositions of *R* and *S* isomers in the solid. The solid line on the circle symbols corresponds to the solubility curve, while the dashed lines connecting the symbols and the bottom line represent tie lines. Point *A* indicates an example to describe crystallization behavior starting at racemic composition. When crystallization started from point *A*, the compositions of the solid phase and solution phase were described by both ends of the tie lines at the thermodynamical equilibrium.

from the (112) plane, which is along the direction between amine molecules in the adjacent columns (Fig. S1, ESI†). These continuous changes suggest that the *S* and *R* enantiomers can substitute each other without impairing the periodicity of the crystal lattice. The overlapped peaks at 16° clearly split into 15.5° and 16.0° with the enrichment of **RL**. These changes occurred continuously, suggesting that the *S*- and *R*-isomers are continuously replaced in the crystal and the overall periodicity is retained. This behavior supports the formation of a solid solution. Similar behavior was observed in the solid solution of racemic salt.[9] These observations in the phase diagram and PXRD measurements indicate that both **SL** and **RL** were incorporated in the same crystal, confirming the formation of a solid solution in the entire composition range.

In order to quantitatively design the chiral resolution process by crystallization using this complete solid solution system, a quasi-ternary isotherm, **SL**/**RL**/methanol, was constructed. After solubility tests with various solvents, methanol was selected for isotherm construction and chiral resolution study due to the moderate solubility of **1**. The construction of the ternary isotherm was conducted by the gravimetric solubility measurement at various compositions. Most of the tie lines connecting the solubility curve and the compositions of deposited crystals did not intersect (Fig. 4), indicating that sufficient thermodynamic equilibrium had been achieved during measurement. The solubility curves can be connected smoothly for all compositions. The compositions of the solution and crystalline phases connected by tie lines are drawn continuously, varying from 0/100 to 100/0. This is a feature of the tie line in a complete solid solution system.[10]

To understand the possible enrichment pathway and potential problems, the crystallization behavior is simulated based on the isotherm. For example, considering a supersaturated solution with an overall composition at point A in Fig. 4b, if crystals precipitate from this solution, the composition of the solution phase is 20.6/79.4 and the crystalline phase is 63.8/36.2 (28% ee) at the thermodynamic equilibrium. Once this equilibrium is achieved, the compositions of the crystalline and solution phases remain constant, although there may be fluctuations due to the dynamic exchange of substances. This means that if crystallization is conducted under these conditions, the maximum optical purity of the crystals at thermodynamic equilibrium is 28% ee. In other words, chiral enrichment is certainly achieved by crystallization in the present system, but the enrichment rate in a single crystallization is small.

This simulation is also confirmed by experiments (Fig. S9, ESI†). Based on the isotherm, the optical purity of the crystals can be gradually increased by repeated crystallization with the appropriate amounts of solvent. When rac-**1** (800 mg) was crystallized from methanol (15 mL), the ee of **1** in the crystal at thermodynamic equilibrium reached 24%. Then, the crystals were collected by filtration and recrystallized from methanol twice. The ee of **1** in the crystals reached 42%. Eventually, we repeated the crystallization four times and the final ee of **1** in the crystals reached up to 80%. These enrichment paths rely on the tie-lines of the isotherm. The ternary isotherm indicates that the ee in the crystal can be gradually enriched by repeated crystallization, even starting from the racemate. However, the yield is very low and the operation time is inefficient.

The steep slope of the tie line in the ternary isotherm inspired enantioselective dissolution as a more efficient enrichment method beyond the limitations given by thermodynamics. The enriched crystalline phase, in thermodynamic equilibrium, is subsequently immersed in a new solvent to selectively dissolve the minor diastereomeric salt. Pioneering work was reported by Levilain and coworkers.[11] They applied enantioselective dissolution in the saturated solution with a single enantiomer during preferential crystallization. In the diastereomeric systems of **SL** and **RL**, **RL** is less stable than **SL** and is expected to show a higher dissolution rate.

The crystals collected at thermodynamic equilibrium, starting from various compositions (20 mg), were immersed in methanol (1.0 mL) at 50 °C and collected after stirring for 5 min. The mass of the crystal and the ee of **1** in the crystalline phase were measured after drying.

Fig. 5 summarizes the enrichment of the ee of **1** in the crystals by enantioselective dissolution. We succeeded in improving the ee of **1** in crystals with a wide range of ee by immersing them in methanol for 5 min, toward the *S*-isomer. Notably, even crystals with an ee as high as 92% could be

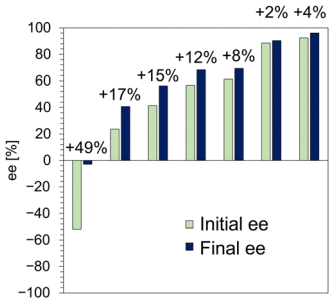

Fig. 5 Enantio-enrichment of **1** by enantioselective dissolution in methanol.

improved to 96% ee in a short time. The amount of enrichment also tended to increase with the amount of *R*-isomer in the initial crystals, *i.e.*, lower initial ee yielded greater enrichment. This observation indicates that the *R*-isomer is selectively eluted from the crystals and its rate increases with the amount of *R*-isomer. The elution rate of the *R*-isomer from **SL** was monitored and a dramatic dissolution occurred in the first 5 min (Fig. S10, ESI†), followed by gradual dissolution over a longer time toward a new thermodynamic equilibrium state. The behavior of the enantioselective dissolution clearly reflects the relative stability of **SL** and **RL**. Consequently, enantioselective dissolution overcomes the limitations of thermodynamics in a short time and is expected to become a powerful technique for chiral resolution of solid solutions.

This study developed a novel chiral resolution method for solid solutions by combining the thermodynamics of crystallization and the kinetics of enantioselective dissolution. The demonstration was conducted with the key intermediate of ZEPOSIA® and di-*p*-toluoyl-L-tartaric acid, which form a complete solid solution. A thorough phase diagram study revealed the limitations of chiral enrichment by crystallization. Further enrichment beyond the thermodynamic limitation was achieved by subsequent enantioselective dissolution. The combination of the crystallization and dissolution processes successfully provided *S*-**1** in excellent optical purity. We believe that this demonstration pioneers a method to rapidly achieve excellent enantioselective purity in solid solution systems. The results offer an innovative solution for engineers and researchers who need to economically pursue process development with limited time and physical resources when encountering solid solutions.

The authors would like to thank Dr K. Hirose for the initial assessment of chiral HPLC analysis with a CD detector. This work is supported by KAKENHI (JP21K20534) from JSPS and a project JPNP20004 by NEDO. I. H. thanks Hoansha for their financial support. R. O. and I. H. thank the Multidisciplinary Research Laboratory System for Future Developments, Osaka University. The PXRD measurement were performed at the Analytical Instrument Facility, Graduate School of Science, Osaka University. Theoretical calculations were conducted through SQUID at the Cybermedia Centre, Osaka University.

Conflicts of interest

There are no conflicts to declare.

Notes and references

1 J. Ding and D. G. Hall, *Angew. Chem., Int. Ed.*, 2013, **52**, 8069–8073.
2 (*a*) L. C. Harfouche, C. Brandel, Y. Cartigny, S. Petit and G. Coquerel, *Chem. Eng. Technol.*, 2020, **43**, 1093–1098; (*b*) A. S. Dunn, B. Szilagyi, J. H. ter Horst and Z. K. Nagy, *Cryst. Growth Des.*, 2020, **20**, 7726–7741; (*c*) F. Cascella, E. Temmel, A. Seidel-Morgenstern and H. Lorenz, *Org. Process Res. Dev.*, 2020, **24**, 50–58; (*d*) F. Zhou, O. Shemchuk, M. D. Charpentier, C. Matheys, L. Collard, J. H. ter Horst and T. Lessens, *Angew. Chem., Int. Ed.*, 2021, **60**, 20264–20268; (*e*) J. Mahieux, M. Sanselme, S. Harthong, C. Melan, C. Aronica, L. Guy and G. Coquerel, *Cryst. Growth Des.*, 2013, **13**, 3621–3631; (*f*) G. Coquerel, R. Bouaziz and M. J. Brienne, *Chem. Lett.*, 1988, 1081–1084.
3 (*a*) F. Zhou, L. Collard, K. Robeyns, T. Leyssens and O. Shemchuk, *Chem. Commun.*, 2022, **58**, 8560–8563; (*b*) M. H. T. Kwan, J. Breen, M. Bowden, L. Conway, B. Crossley, M. F. Jones, R. Munday, N. P. B. Pokar, T. Screen and A. J. Blacker, *J. Org. Chem.*, 2021, **86**, 2458–2473; (*c*) N. Uemura, Y. Yoshida, T. Mino and M. Sakamoto, *Tetrahedron*, 2020, **76**, 131166; (*d*) D. F. Bánhegyi, D. Szolcsányi, J. Madarász and E. Pálovics, *Chirality*, 2022, **34**, 374–395; (*e*) L. Marc, S. Guillemer, J.-M. Schneider and G. Coquerel, *Chem. Eng. Res. Des.*, 2022, **178**, 95–110.
4 (*a*) M. Guillot, J. de Meester, S. Huynen, L. Collard, K. Robeyns, O. Riant and T. Leyssens, *Angew. Chem., Int. Ed.*, 2020, **59**, 11303–11306; (*b*) W. Li, M. De Groen, H. J. M. Kramer, R. Gelder, P. Tinnemans, H. Meekes and J. H. ter Horst, *Cryst. Growth Des.*, 2021, **21**, 112–124; (*c*) O. Shemchuk, F. Grepioni, T. Leyssens and D. Braga, *Isr. J. Chem.*, 2021, **61**, 563–572.
5 (*a*) K. Sanada, A. Washio, H. Ishikawa, Y. Yoshida, T. Mino and M. Sakamoto, *Angew. Chem., Int. Ed.*, 2022, **61**, e202201268; (*b*) R. Oketani, F. Marin, P. Tinnemans, M. Hoquante, A. Laurent, C. Brandel, P. Cardinael, H. Meekes, E. Vlieg, Y. Geerts and G. Coquerel, *Chem. – Eur. J.*, 2019, **25**, 13890–13898; (*c*) G. Valenti, P. Tinnemans, I. Baglai, W. L. Noorduin, B. Kaptein, M. Leeman, J. H. Ter Horst and R. M. Kellogg, *Angew. Chem., Int. Ed.*, 2021, **60**, 5279–5282.
6 E. Martinborough, M. F. Boehm, A. R. Yeager, J. Tamiya, L. Huang, E. Brahmachary, M. Moorjani, G. A. Timony, J. L. Brooks, R. Peach, F. L. Scott and M. A. Hanson, *Selective Sphingosine 1 Phosphate Receptor Modulators and Combination Therapy Therewith*, 2015, 2015066515A1.
7 F. Uthoff, J. Löwe, C. Harms, K. Donsbach and H. Gröger, *J. Org. Chem.*, 2019, **84**, 4856–4866.
8 C. Cianferotti, G. Barreca, V. Bollabathini, L. Carcone, D. Grainger, S. Staniland and M. Taddei, *Eur. J. Org. Chem.*, 2021, 1924–1930.
9 A. Mbodji, G. Gbabode, M. Sanselme, Y. Cartigny, N. Couvrat, M. Leeman, V. Dupray, R. M. Kellogg and G. Coquerel, *Cryst. Growth Des.*, 2020, **20**, 2562–2569.
10 In the case of eutectic systems, solubility increases at the eutectic composition and the crystalline phase is of a single composition when the composition in solution changes. Further details of the phase diagram of eutectic systems are described in the following reviews. (*a*) G. Coquerel, *Polymorphism in the Pharmaceutical Industry*, Wiley-VCH Verlag GmbH & Co. KGaA, Weinheim, Germany, 2018, pp. 91–132; (*b*) G. Coquerel, in *Advances in Organic Crystal Chemistry: Comprehensive Reviews*, ed. R. Tamura, M. Miyata, Springer Japan, Tokyo, 2015, pp. 393–420.
11 G. Levilain, M. J. Eicke and A. Seidel-Morgenstern, *Cryst. Growth Des.*, 2012, **12**, 5396–5401.

